Protein-Based Microfluidic Models for Biomedical Applications

Joe Tien and Yoseph W. Dance

Contents

Abstract

Protein-based microfluidic extracellular matrices (ECMs) are naturally well-suited as templates for the creation of perfusable microvessels and epithelial tubes. By definition, microfluidic ECMs contain open and/or blind-ended channels with diameters on the order of 100 μm or smaller. They are designed to be

J. Tien (✉)
Department of Biomedical Engineering, Boston University, Boston, MA, USA

Division of Materials Science and Engineering, Boston University, Boston, MA, USA
e-mail: jtien@bu.edu

Y. W. Dance
Department of Biomedical Engineering, Boston University, Boston, MA, USA

immediately perfusable, and thus do not rely on biological tubulogenesis to form lumens. Methods to create the microfluidic networks can be applied to a broad range of matrix compositions and network geometries and topologies. When lined by a monolayer of endothelium or epithelium, a microfluidic ECM can be converted into a microvascular or epithelial model. Introduction of substances or cells through the lumen of such models enables study of transport properties and the biophysical and biochemical factors that control these properties. Microfluidic models can also be used to analyze, predict, and optimize the design of micro-fluidic networks within engineered tissues.

Introduction

In vivo, the extracellular matrix (ECM) is *microstructured*. That is, the matrix contains features that display heterogeneity over lengths on the order of 10–100 μm, which is comparable to the size of the smallest multicellular organizations within a tissue. For instance, blood vessel capillaries and renal tubules are approximate cylinders with diameters of 5–10 μm and 30–40 μm, respectively, while lung alveoli and renal glomeruli are approximate spheres with diameters of 100–300 μm. Removal of the living components in a tissue through decellularization readily reveals the micro-structured geometry of the ECM. This microstructure is distinct from the nanometer-scale, pore-level ultrastructure.

Reconstruction of tissue structures in vitro is often performed with protein-based matrices as a scaffold for cell culture. Given the microstructured nature of ECM in vivo, one naturally expects that using a geometrically heterogeneous matrix as a scaffold could be advantageous over using a homogeneous one. Many studies over the last two decades have validated this idea, with microstructured ECMs serving as scaffolds for modeling of tissue physiology, development, and dysfunction (Nelson and Tien 2006; Tien and Nelson 2014). These studies often apply poly-dimethylsiloxane (PDMS) elastomer-based micropatterning technologies (McDonald and Whitesides 2002), suitably adapted for micromolding of collagen- and other protein-rich hydrogels (Nelson et al. 2008; Tang et al. 2003), to create the desired matrix microstructure.

One area where the development of such patterned ECMs has advanced tremen-dously is in the creation of microfluidic networks within the bulk material and in the use of these so-called "microfluidic biomaterials" as cell culture scaffolds (Stroock and Cabodi 2006; Tien and Dance 2021). By definition, the microstructure that characterizes this class of ECMs consists of open and/or blind-ended channels or interconnected networks that can span the width of the scaffold. Microfluidic ECMs are inherently perfusable, a property that underlies much of the interest in these
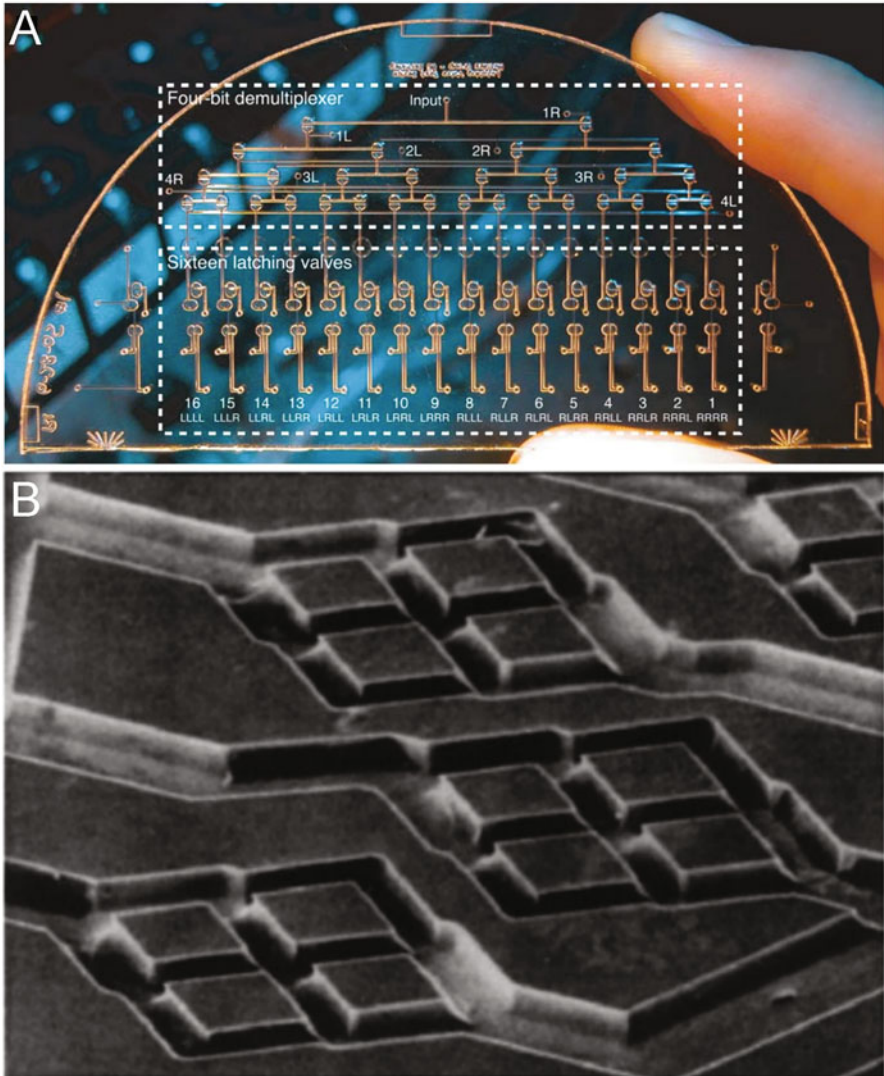
Fig. 1 PDMS-based microfluidic technology and its extension to other types of materials. (**a**) PDMS device with large-scale microfluidic integration. (Reproduced with permission from Grover et al. 2006). (**b**) Degradable polymer-based microfluidic array that mimics the vasculature. (Reproduced with permission from Borenstein et al. 2002)

biomaterials. Given the geometric complexity of devices that have been developed using conventional microfluidics with PDMS (Fig. 1a) (Melin and Quake 2007), the hope of many research groups is to replicate such success in protein-based biomaterials.

Seminal work by Vacanti and colleagues proposed that microfluidic ECMs, designed in silico, could be used to grow microfluidic tissue structures (Fig. 1b) (Kaihara et al. 2000). These authors intended to use the microfluidic networks as templates to create open microvascular networks and for good reason: fluid and solute transport within engineered tissues was (and still remains) the key obstacle toward translating advances in biomaterials synthesis into the creation of viable critically-sized tissue implants. The ability to create open vascular networks within biomaterials could ameliorate such transport issues. Although Vacanti's original concept targeted vascular networks, many other types of transport structures within tissues (e.g., renal tubules, glandular ducts) could also benefit from being formed within microfluidic biomaterials. Many of the same tissue structures that were envisioned for implantation have found an enthusiastic audience and more immediate application in the field of microphysiological systems, where the microscale tissues provide a simplified, perfusable analog of a human tissue.

This chapter of the handbook covers the synthesis and application of microfluidic ECMs for biomedical models. The examples in this chapter focus on protein-based matrices; microfluidic scaffolds that do not consist of proteins are noted when appropriate. The immense practical advantages of the microfluidic approach to vascularization have led to most applications being developed for creating open microvessels, and the chapter devotes the largest section to this application. As noted above, nonvascular tubular structures exist in vivo; the formation of epithelial tubes in microfluidic ECMs is addressed here as well. For the reader who is interested in purely technical details, consultation with protocols that provide step-by-step instructions on how to make and use microfluidic scaffolds is highly encouraged (Price and Tien 2009, 2011).

Outside the scope of this chapter is the discussion of microfluidic devices that only contain adsorbed matrix proteins, such as in many recent implementations of organs-on-a-chip (Huh et al. 2010), or geometrically unpatterned (i.e., bulk) ECM. Recent advances in three-dimensional (3D) printing technologies will only be addressed in passing, and the interested reader is directed to the chapters by Wang and by Hajiabbas et al. in this handbook.

Synthesis of Microfluidic Protein-Based Biomaterials

Unlike synthetic polymers, protein-based matrices do not form by covalent polymerization and cross-linking of low-molecular-weight organic precursors. Instead, these biomaterials form by self-assembly of monomeric proteins into fibrils and fibers that pass a percolation threshold and then entangle into porous hydrogels. Patterning microfluidic networks in such protein-based scaffolds requires careful attention to the modest mechanical stiffness and thermal stability of these materials. Many suitable methods have been developed, and they can be broadly categorized as "subtractive" or "additive."

Subtractive Approaches

A subtractive micropatterning technique is one in which the final structure is built around a temporary patterning element that is eventually removed. For example, the use of photoresists in standard photolithography is often part of a subtractive process: the patterned resist serves as a sacrificial element to enable patterning of other types of materials, such as metals or ceramics. Because protein-based scaffolds are not stable enough to withstand harsh chemical treatments that can remove photoresist, standard processes in lithography cannot be directly applied to these materials. Gentler subtractive methods that preserve the bioactivity of the ECM have been developed (Price and Tien 2009).

The simplest method of removing a sacrificial element is mechanical. For instance, collagen-based microfluidic ECMs can be formed by gelation of a neutralized solution of type I collagen monomer around a thin metal or glass needle and mechanical removal of the needle (Fig. 2a) (Chrobak et al. 2006; Linville et al. 2016). If the liquid precursor is added only around the central portion of the needle, then the resulting scaffold has an open channel. If the precursor also covers the distal end of the needle, then the resulting scaffold has a blind-ended channel. In this strategy, the templating element need not be rigid. Deformable Y-shaped PDMS microstructures have been used in an analogous manner to form Y-shaped branched channels within type I collagen gels (Jiménez-Torres et al. 2016).

The advantage of this mechanical approach is its simplicity. One can be confident that the final scaffold does not contain any residue from the patterning element. The pore structure of the patterned matrix resembles that of bulk material that is cast in a plastic cell culture dish. The disadvantage is that as the desired channel sizes become smaller, the required needle or template may become so narrow that it becomes flimsy, and mechanical removal may not be feasible. Practically, channels with diameters as small as 20–30 μm can be formed with this approach. A second disadvantage is that this approach is limited to simple microfluidic network topologies, such as channels and Y-shaped junctions.

Another sacrificial approach is based on removing the patterning element by dissolving it. Gelatin gels have the useful property of melting near 37°C, which is not high enough to compromise the structure of collagen-based gels. Micropatterned gelatin meshes can thus be used as a sacrificial element that, upon removal by melting, yield microfluidic collagen gels that contain interconnected microfluidic networks (Golden and Tien 2007). Conversely, aqueous solutions of Pluronic poly (propylene oxide)-poly(ethylene oxide)-poly(propylene oxide) copolymers form gels that liquefy below a critical temperature. These solutions can be extruded at high temperature as sacrificial "inks" that can be encapsulated in an ECM and then removed under low temperature (Kolesky et al. 2014). Another suitable sacrificial material is sugar-based filament, which dissolves readily in aqueous solutions (Miller et al. 2012). Gelatin, Pluronic, and sugar-based inks have all been adapted for use in 3D-printing instruments, which provide unparalleled versatility in the

Fig. 2 Examples of microfluidic protein-based biomaterials. (**a**) Type I collagen gel with a single channel, formed subtractively. (Reproduced with permission from Chrobak et al. 2006). (**b**) Alginate gel with an array of interconnected channels, formed additively. The interface between the bonded alginate objects is still visible in the cross-sectional view. (Reproduced with permission from Cabodi et al. 2005). (**c**) Organ-scale ECM from perfusion-decellularization of a pig heart. (Reproduced with permission from Ott et al. 2008). Scale bars refer to 100 μm in (**a**) and 500 μm in (**b**)
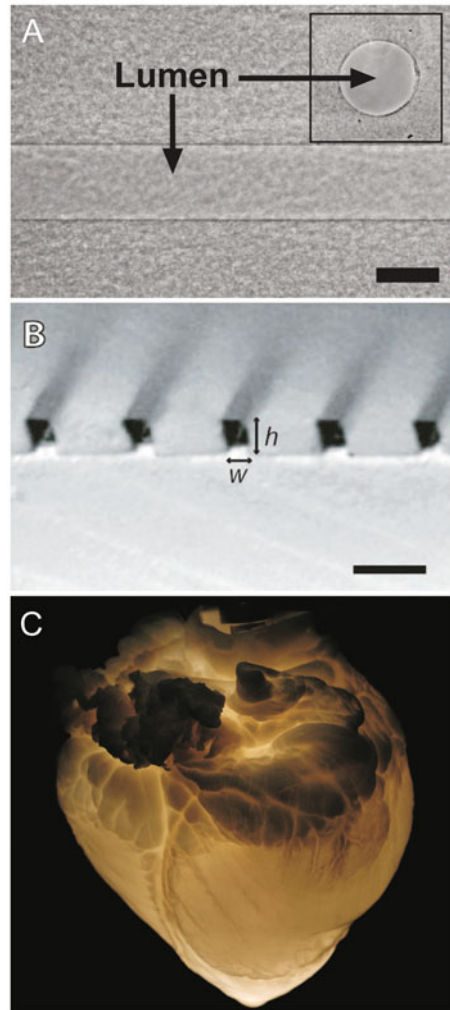
topology of the resulting microfluidic architecture. Micromolded gelatin can yield channels as narrow as 5 μm, while 3D-printed inks have substantially coarser resolution.

A third sacrificial approach is based on using a fluid mechanical phenomenon, known as the Raleigh-Taylor instability, to pattern the ECM. This instability results in "viscous fingering," in which a a pressurized fluid of lower viscosity (typically, saline) forms a fluid stream in a liquid ECM precursor of higher viscosity (Bischel et al. 2012). Once the precursor is set, the fluid stream becomes the channel within

the scaffold. Viscous fingering does not require mechanical or chemical removal of a template and thus is unusually simple to implement. The trade-off for the ease of use is that the geometry of the resulting channels is largely constrained by external boundary conditions (e.g., fluid pressure, dimensions of the ECM-containing volume). Channel diameters are typically much larger than 100 μm.

Finally, although protein-based matrices are not intrinsically photosensitive, they can absorb high-intensity light that ablates the fibers within a narrow spot. Pulsed laser-based systems can draw channels within a bulk ECM voxel-by-voxel (Ilina et al. 2011). At higher intensities, laser pulses induce gas bubbles by cavitation of pore fluid within bulk matrix; dragging these bubbles through the matrix can also be used to generate channels (Enrico et al. 2022).

Additive Approaches

Additive approaches do not build a scaffold around a sacrificial element. Instead, they construct the desired structure "brick by brick" by arranging individual matrix structures into a 3D assembly and then welding them into a cohesive whole. The first demonstration of this approach to create a microfluidic biomaterial was in alginate gels (Fig. 2b) (Cabodi et al. 2005). Although not a protein, alginate can also be micropatterned with high resolution. Microfluidic networks can be constructed by pressing a flat gel onto a patterned one that contains recessed features in the shape of a network. This strategy is particularly suitable for micromolding techniques and has been applied extensively with type I collagen gels (Zheng et al. 2012). Because the individual patterns are typically molded using PDMS structures, the sidewalls of the channels are vertical, and the resulting channels have rectangular cross sections.

Most ECM gels can exhibit some degree of passive adhesion, but if the channels are to be maintained under pressure (e.g., for pumping fluid), then methods to increase the inter-gel adhesive strength are important. The most common strategy is to transiently and partially depolymerize and then quickly re-polymerize the gels so that some fibers re-form across the gel-gel interface, thereby mechanically entangling the gels. With alginate, such cycles of de-/re-polymerization can be induced by transient treatment with the calcium ion chelator citrate (Cabodi et al. 2005). With collagen and fibrin gels, transient exposure to chaotropic agents such as urea is sufficient (Price et al. 2008). Although the starting gel-gel interface cannot be completely erased by this approach, the interfacial adhesive strength can be increased so that it is comparable to the strength of a bulk gel. Silk fibroin scaffolds can be bonded by transient exposure to high temperatures that melt and then re-solidify the biomaterial at the interface (Bettinger et al. 2007).

Microfluidic ECMs can also be formed by additive printing of a liquid ink that solidifies immediately upon release (Hinton et al. 2015; Lee et al. 2019). The speed of the gelation process and the rheology of the bath into which the ink is printed control the achievable spatial resolution.

Approaches That Use Biologically Derived Patterns

Despite the tremendous sophistication of existing micropatterning techniques that use PDMS molds or 3D printers, the geometric complexities of the resulting scaffolds do not yet match those found in vivo. One method to obtain microfluidic ECMs that essentially replicate in vivo microfluidic architectures is perfusion decellularization (Fig. 2c) (Badylak et al. 2011; Ott et al. 2008). This technique decellularizes a whole organ by perfusing its vasculature with surfactant-rich solution. The result is an organ-scale scaffold that contains a microfluidic network in the shape of the original microvascular network. Both animal- and plant-derived tissues have been used as starting material (Gershlak et al. 2017). To date, perfusion-decellularization has been used to generate large scaffolds for implantation, although biopsies of these scaffolds could in principle be used in microphysiological systems.

Microfluidic ECMs in Models of the Microvascular System

The original motivation for the development of microfluidic protein-based ECMs was to create perfusable microvessels, both for vascularization of implantable tissues and for modeling of human microvascular physiology, in a process termed "microfluidic vascularization" (Tien 2014). To date, these scaffolds have found much more application in microvascular models than in implants. In vivo, the blood-containing microvascular system is a hierarchical network that consists of arterioles, capillaries, and venules (Wiedeman 1984). Segments of a microvascular network are all lined by a monolayer of endothelial cells but vary in the organization of their surrounding mural cells (smooth muscle cells and pericytes). Vessels are embedded within an interstitium that contains collagen-rich ECM and mesenchymal cells, such as fibroblasts and adipocytes. The architecture of microvascular networks varies greatly by organ, as can be seen in corrosion casts (Fig. 3) (Kessel and Kardon 1979). When using microfluidic ECM to form models of the microvascular system, one should consider to what extent such organ-specific vascular geometries need to be replicated for the application of interest. This consideration is especially important given that micropatterning techniques are not yet sufficiently advanced to perfectly reproduce in vivo microfluidic architectures. In general, microfluidic vascularization has required a channel on the order of 10–100 μm in diameter, a lining of endothelium, and an open lumen that can sustain flow.

A separate microvascular network in vivo comprises the lymphatic system (Breslin et al. 2018). Lymphatic microvessels consist of initial capillaries and collecting lymphatics. In contrast to the main (blood-containing) microvascular system, the lymphatic system has a tree-like topology, with the lymphatic capillaries being blind-ended rather than being open at both ends. These blind ends serve as the interface between the surrounding interstitium and the lymphatic lumen.

Given the pervasiveness of microvessels in nearly all organs, it is not surprising that the microvasculature plays a critical role in the progression of virtually all human diseases. Among the diverse functions that microvessels provide are serving

Fig. 3 Corrosion casts of microvascular networks from (**a**) thyroid gland and (**b**) small intestine. (Reproduced with permission from Ohtani et al. 1983)
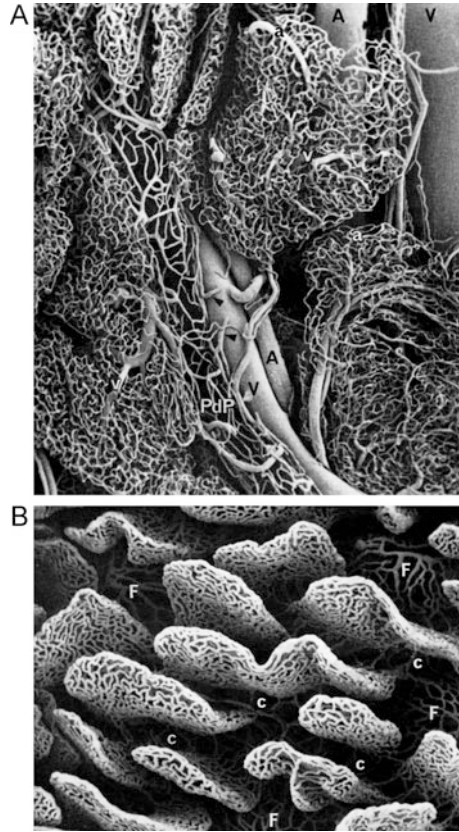
as a transport barrier between the bloodstream and interstitium, autoregulation of blood transport, maintenance of blood fluidity, biochemical transformation of blood-borne substances, drainage of interstitial fluid and cells, regulation of leukocyte adhesion and the inflammatory response, antigen presentation, and many others (Zweifach 1973). These functions can be quantified with physiological metrics, such as permeability coefficients, which allows direct comparison of the functionality of in vivo microvessels with that of engineered ones in an in vitro model (Yuan and Rigor 2011). For further information on microvascular anatomy and physiology, the reader is highly encouraged to consult the chapters on microcirculation in the current and older editions of the *Handbook of Physiology*.

Transformation of Microfluidic Channels into Microvessels

To convert the channels in a microfluidic ECM into microvessels, one typically introduces a suspension of endothelial cells (ECs) into the channel by flow (Chrobak

et al. 2006). Although ECs often exist in vivo on a laminin- and type IV collagen-rich basement membrane, they attach and spread well on type I collagen, which is the main ECM that has been used in microfluidic models. Under optimized conditions, the seeded ECs proliferate and eventually form a single-layer tube that serves as an in vitro analog of a native microvessel.

The scaffold must promote cell spreading and proliferation, as the seeding step usually leads to non-uniform distribution of a limited number of cells in the channel. Type I collagen and fibrin are suitable substrata, as are ECMs that contain mixtures of type I collagen and other proteins (fibronectin, type IV collagen, laminin). Without the inclusion of type I collagen, a basement membrane gel of type IV collagen and laminin does not support EC spreading and has not been shown to support microfluidic vascularization. Whether this problem arises from biochemical signaling peculiar to type IV collagen- and laminin-mediated cell adhesion, or from the low stiffness of basement membrane gels, is unclear. In general, the stiffer the matrix, the more suitable it is as a substratum for endothelialization (Fig. 4a) (Chan et al. 2014; Chrobak et al. 2006).

Microfluidic ECMs are porous at two size scales: that of the channels (typically 5–100 μm in diameter) and that of the ECM itself (as governed by the density of matrix fibers). Formation of morphologically stable microvessels requires that the pore size of the ECM proper should be small enough to restrict the migration of ECs (Fig. 4b) (Chrobak et al. 2006). One should keep in mind the difference between pore size and "porosity," the latter being the fluid volume fraction; two scaffolds of the same porosity can have wildly different pore sizes. It is pore size, not porosity, that controls the interstitial migration of ECs. Measurement of the ECM hydraulic permeability can yield a rough estimate of the average pore size. For more detailed structural analysis, the distribution of pore sizes can be assessed through scanning electron microscopy or optical imaging (Raub et al. 2007). When pore sizes in the

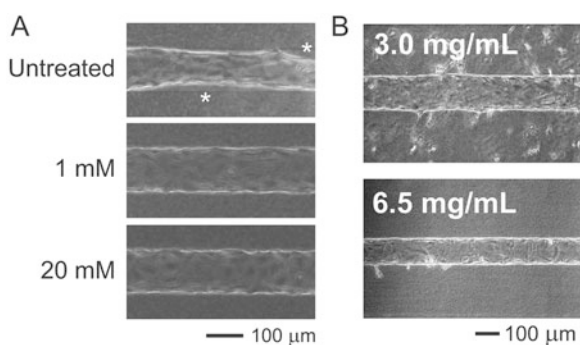**Fig. 4** Role of scaffold properties in success of endothelialization of microfluidic biomaterials. (**a**) Cross-linking of ECM with 1 mM or 20 mM genipin increases endothelial stability. (Reproduced with permission from Chan et al. 2014). (**b**) Larger ECM concentration (6.5 mg/mL type I collagen) results in smaller pore size and lower levels of endothelial cell invasion. (Reproduced with permission from Chrobak et al. 2006)

bulk matrix are on the order of micrometers, ECs can migrate from the channel into the pore space; although this process resembles sprouting angiogenesis in vivo, it is driven purely by pore architecture and not by angiogenic growth factors.

Special consideration is needed when using microfluidic ECMs to form capillaries, since individual ECs are too large to disperse through capillary-scale channels. At this scale, one forms vessels by promoting the distal migration of ECs along the channel walls (Linville et al. 2016). This migration can be induced by flow in the opposite direction, since ECs migrate against the direction of flow (Ostrowski et al. 2014). Alternatively, one can simply wait for ECs to migrate on their own in the absence of external stimulation (Arakawa et al. 2020; Qiu et al. 2018). Either way, "capillaries" as narrow as ~20 μm have been formed and perfused. In contrast to microvascular networks that form via in vitro angiogenesis or vasculogenesis, these capillaries have a reproducible geometry and are readily perfused.

Physical Factors in Microfluidic Vascularization

Many studies in microfluidic vascularization have focused on the role of physical factors, such as flow and shear stress, in the functionality of the resulting vessels. This focus on physical factors stems from an appreciation that the vascular system is particularly sensitive to its mechanical microenvironment. Endothelium is chronically exposed to, and responds to, pulsatile pressure and flow in vivo, even in the lymphatics; one expects similar behavior in engineered systems.

The overall balance of physical stresses at the matrix-endothelium interface appears to govern the long-term stability of microvascular networks within a microfluidic ECM (Fig. 5) (Wong et al. 2014). This balance results from the interplay of at least three distinct stresses. First, the transmural or trans-endothelial pressure P_{TM} (i.e., the difference between the pressure within the vessel lumen and the pressure in the surrounding matrix) serves to stabilize the endothelium (Wong et al. 2013). Second, the cell contractility-induced Laplace stress $\sigma \equiv \gamma/r$ serves to destabilize the

Fig. 5 Balance of physical factors in vascularization of microfluidic biomaterials. $P_{scaffold}$, pore pressure within ECM; P_{lumen}, fluid pressure within channel (equivalent to P_{vessel} in Figure 7); γ_{EC}, endothelial contractility; σ_{adh}, cell-ECM adhesion stress; r, channel radius. (Reproduced with permission from Wong et al. 2014)
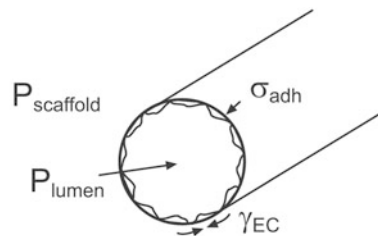
Condition for stability: $P_{lumen} - P_{scaffold} > \dfrac{\gamma_{EC}}{r} - \sigma_{adh}$

endothelium; here, γ refers to the EC contractility (akin to a surface tension), and r is the vascular radius. Third, the matrix-endothelium adhesive stress σ_{adh} promotes stability. These stresses can be arranged in an inequality that must be satisfied for vascular stability to be obtained:

$$P_{TM} + \sigma_{adh} > \frac{\gamma}{r}$$

When this inequality is violated, endothelial cells can detach as individual cells or as entire patches from the channel walls.

The idea of a stress balance can be used to explain why a given microfluidic operating condition is stabilizing or destabilizing. For instance, as mentioned previously, scaffolds of greater stiffness are more suitable for endothelialization. While this effect partly results from improved EC spreading on a stiff matrix, the adhesive stress σ_{adh} also increases with stiffness, which leads to greater stability. Similarly, the inclusion of a blind-ended channel within the matrix, separate from the vessel and held at low pressure, reduces the fluid pressure within the pores of the ECM that surrounds the vessel (Wong et al. 2013). Lowering the pore pressure increases the transmural pressure P_{TM} and thus stabilizes the vessel. The contractility-induced stress γ/r has been manipulated by "relaxing" the endothelium with cell-permeant drugs that interfere with actin-based cell contractility. Such drugs include the phosphodiesterase inhibitor Ro-20-1724 and the ROCK inhibitor Y-27632, which decrease the traction forces exerted by ECs on the scaffold, cause the endothelial tension to decrease, and improve vascular stability (Linville et al. 2019; Wong et al. 2010).

Barrier function, one of the main microvascular functions, responds to both acute and chronic levels of physical stress. Studies of barrier function in microfluidic vascularization have revealed an unexpected link between the leakiness of the vascular barrier and the stability of EC adhesion to the matrix. For a vessel of a given diameter, a slower intravascular flow rate results in a leakier barrier, which can be revealed by perfusing the vessel with fluorescently labeled solutes (Price et al. 2010). These experiments can be used to calculate effective solute permeability coefficients that can be compared to previously measured benchmarks from microvessels in vivo. The endothelial barrier responds to levels of shear stress, and not flow rate per se, with a sharp transition from leaky to tight barrier function occurring at a shear stress of 15–20 dyn/cm^2.

Whether induced by a higher shear stress or by a different signal (e.g., inhibition of phosphodiesterase), a stronger vascular barrier is invariably accompanied by greater vascular stability. This finding can be rationalized by the ability of leaks within the vessel wall to raise the fluid pressure within the matrix pores. Much as a balloon can be deflated by puncturing its wall with a pinprick, the endothelium can be destabilized from the ECM by the formation of a tiny (<1 μm) leak between EC junctions. In general, any substance that increases the organization of EC junctions results in a stronger barrier and greater stability (Leung et al. 2012; Wong et al. 2010).

Models of Microvascular Activation

Much of the power in using these vascular models lies in the high reproducibility of the vascular geometry: large numbers of vessels of nearly identical diameters and lengths can be formed in microfluidic ECMs, which removes vascular geometry as a potential confounding factor. Given the importance of the vascular barrier, it is not surprising that vessels within a microfluidic ECM have been used as models of barrier function and breakdown. For instance, the opening of the blood-brain barrier (BBB) with hyperosmotic mannitol can be studied in this system (Linville et al. 2020). Although the use of mannitol to transiently disrupt the BBB is clinically important for drug delivery to the brain parenchyma, such disruption is appreciated at a gross level, and the underlying local mechanisms have been poorly explored. With a microfluidic model of the BBB, the status of the endothelial barrier can be visualized across an entire vessel and in real time. Breakdown of the barrier manifests both as a generalized loss of barrier function and as localized "focal leaks" that allow escape of solute from the vessel lumen into the surrounding matrix. The vascular model can also be used to test other agents for their efficacy in BBB disruption (Linville et al. 2021). Similar work has shown that plasma expanders, which are used clinically to restore plasma volume in critical fluid loss and to promote organ viability in hypothermic organ preservation, improve the vascular barrier in a non-BBB model (Leung et al. 2012). In all of these examples, it is perhaps not coincidental that changes in vascular barrier occur mainly when clinically active drug concentrations are applied.

Other aspects of vascular activation, such as the acute inflammatory response, can be explored using these microfluidic models. Inflammation leads to loss of barrier function and a "stickier" endothelium that supports leukocyte and platelet adhesion. Microfluidic vascular models support leukocyte adhesion, but only when they are inflamed (e.g., with tumor necrosis factor α) (Chrobak et al. 2006). Similarly, activation of vessels with the phorbol ester PMA causes the endothelium to expose von Willebrand factor on its apical surface (Zheng et al. 2012). The tethered protein stretches under flow and supports the adhesion of platelets. Under baseline conditions, little-to-no platelet adhesion is evident.

Vascular models have also been used to study the role of physical factors in angiogenesis. Blood flow is well-appreciated as an angiogenic signal in vivo, but the underlying mechanisms are unclear. Changes in blood flow can result in simultaneous changes in vascular shear stress and pressure, and the latter can cause changes in transmural pressure. Vascular models allow separate control over these factors to enable one to uncover which one(s) promote angiogenesis. Separate control over transmural pressure requires the addition of a separate channel that maintains the ECM pores at a different pressure than the vascular pressure. This channel can be blind-ended (Wong et al. 2013) or open at both ends (Nguyen et al. 2013; Price et al. 2010). Studies in these vascular models have shown that increased flow promotes angiogenesis via an increase in shear stress, but only in the absence of a concomitant rise in transmural pressure (Price et al. 2010). Transmural flow (i.e., across the

endothelium and into the pores of the scaffold) can also promote angiogenesis at supra-physiological levels (Galie et al. 2014).

Microfluidic models of barrier function, inflammation, and angiogenesis generally use vessels with diameters on the order of 100 μm, which is substantially larger than those of venules. In vivo, breakdown of the barrier and sprouting of ECs primarily take place in post-capillary venules. Despite this difference, the larger diameters in engineered models have not proven to be disadvantageous. In fact, they enable higher flow rates for the same axial pressure drop, which allows faster introduction of solutes into the vessel lumen (e.g., during a solute permeability measurement). Moreover, visualization of the side profile of the vessel is easier in larger vessels. When modeling microvascular obstruction (e.g., in sickle cell anemia), the vessels should be narrower; for these applications, capillary-scale vessels can be made in microfluidic ECMs that have appropriately narrow channels (Arakawa et al. 2020; Qiu et al. 2018).

Models of Microvascular Transport and Drainage

Microfluidic models can be used not only to study microvascular processes that are difficult to disentangle in vivo, but they can also help guide the design of engineered tissues for implantation. To achieve clinical relevance, engineered tissues must achieve a minimum tissue size that far exceeds the scale of microfluidic models. Nevertheless, the design of the tissue can be tested at the microfluidic scale, by building a basic "building block" of the tissue and studying its behavior under perfusion. Much of this work has focused on the concept of the Krogh cylinder, in which each vessel delivers oxygen and other solutes to a sleeve of surrounding tissue. In effect, the design of engineered tissues can be simplified to the creation of numerous non-overlapping Krogh cylinders that together comprise the tissue. Measurement of the radius of well-perfused tissue (the "Krogh radius") as a function of perfusion conditions, ECM pore size, vessel radius, and other microfluidic operating conditions enables proper spacing of the channels in the microfluidic ECM and of the vessels in the resulting tissue.

The first studies in this area analyzed solute efflux from unseeded channels instead of from vessels (Choi et al. 2007; Song et al. 2009). For small solutes (e.g., oxygen), transport is dominated by diffusion and is unlikely to be significantly affected by whether or not a channel is lined by endothelium. For large solutes (e.g., proteins), advective transport becomes more important, and the presence of endothelium can greatly alter the rate of vessel-to-tissue transport. Theoretical considerations suggest that when flow within the channel is fast enough, the Krogh radius r_{Krogh} is independent of position along the channel axis and scales in the following way:

$$r_{Krogh} \sim \sqrt{\frac{Dc_0}{R}}$$

where D is the solute diffusivity, c_0 is the solute concentration in the perfusate, and R is the volumetric solute consumption rate in the cell-laden matrix that surrounds the channel. When flow within the channel is rate-limiting, the Krogh radius will decrease downstream.

Studies with unseeded channels and with vessels have largely validated these predictions (Choi et al. 2007; Li et al. 2019; Song et al. 2009). Such predictions can be tested when the solute consumption rate R is unknown and even when the identity of the limiting solute is unknown. By altering the density ρ of parenchymal cells embedded within the matrix, one can vary the volumetric consumption rate, since it is expected to be proportional to cell density. The expected scaling relation is thus $r_{Krogh} \sim \rho^{-1/2}$. By defining a marker of tissue "health," one can infer r_{Krogh} from the distribution of that marker as a function of distance from the channel or vessel wall. For instance, in a model of perfusable and vascularized adipose tissue, adipocytes are embedded within the microfluidic ECM. The health of the parenchymal compartment can be assessed by the degree to which adipocytes accumulate lipid. One expects these data to collapse onto a master curve of lipid content per cell versus $\rho^{1/2}r$, which matches experimental findings (Li et al. 2019).

Transport within engineered tissues is also assessed by the ability of the tissue to be drained by lymphatic vessels or lymphatic-like channels (Fig. 6). As described previously, unseeded blind-ended channels within a microfluidic ECM can stabilize neighboring vessels by lowering the fluid pressure within the pores of the matrix (Fig. 6a) (Wong et al. 2013). These same channels can also provide a route for excess fluid or solute to be removed from the tissue. As with oxygenation and perfusion, here the microfluidic model provides a means to test lymphatic designs in a small-scale format before scaling up the tissue to clinically relevant dimensions. In vivo
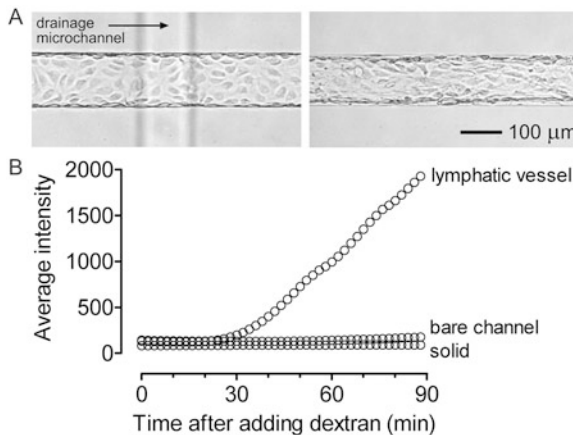

Fig. 6 Microfluidic models of lymphatic function. (**a**) Acellular, lymphatic-like channels promote vascular stability in a microfluidic fibrin gel. (Reproduced with permission from Wong et al. 2013). (**b**) Endothelialized lymphatics promote drainage of fluorescently labeled dextran in a type I collagen gel, as measured by an increase in fluorescence intensity at the downstream end of the gel over time. (Reproduced with permission from Thompson et al. 2018)

measurement of lymphatic functionality consists of injecting a dye or radiolabeled solute into the tissue space and then observing the removal of the solute from the space over time. In models of lymphatic drainage, one can similarly introduce a bolus of fluorescently labeled solute into the ECM and observe its removal from the matrix via the lymphatic that it contains. Because a lymphatic can be visualized along its entire axis, whether lower-than-expected drainage rates result from selective blockage at one part of the vessel or from generalized loss of drainage function can be elucidated.

These lymphatic models have shown that fluid and solute drainage from type I collagen scaffolds are affected differently by the presence of lymphatic endothelium (Fig. 6b) (Thompson et al. 2018). When operated under physiological flow conditions, in which the lymphatic pressure is lower than the pressure in the ECM, the lymphatic vessel exhibits two barrier phenotypes. Upstream (i.e., near the blind-end of the vessel and near the tissue volume to be drained), the lymphatic endothelium is extremely leaky. Downstream (i.e., along the vessel itself), the endothelium is less leaky. As a result, fluid drainage rates are independent of the presence of endothelium; functionally, the endothelium provides no resistance to flow into the lumen. In contrast, solute drainage rates are increased in lymphatics versus in unseeded blind-ended channels. Segmental differences in barrier phenotype allow solutes to enter the lumen near the blind end of the lymphatic, but these solutes are largely retained within the lumen during their transport along and out of the vessel. Ultimately, these segmental differences result from nonlinear flow properties of the lymphatic endothelium, in which the endothelial hydraulic resistance is a strongly nonlinear function of trans-endothelial flow speed. An analog of the Krogh radius, but for drainage, could simplify the design of lymphatic systems that imbue engineered tissues with sufficient drainage capacity.

Computational Design of Microfluidic ECM for Vascularization

The controlled scaffold geometry in microfluidic vascularization lends itself to computational modeling, which complements experimental studies in several ways. First, many parameters of interest (e.g., interstitial fluid or solid pressure in the ECM, pressure within a channel or vessel) either cannot be measured directly or can only be obtained by severely altering the microfluidic system. Computational models enable one to estimate difficult-to-measure quantities and how they vary across the scaffold and channel or vessel volume. Second, computational models allow one to test any assumptions that underlie the microfluidic operation. For instance, it is generally assumed that the regions of bulk ECM are isotropic after patterning. Any discrepancy between computational predictions and experimental observations can indicate the invalidity of such assumptions. Third, computational models allow one to rapidly screen different microfluidic operating conditions for a desired output. Once a baseline model is confirmed to largely reproduce experimental findings, it is faster to optimize vascular function by altering the microfluidic geometry, flow conditions, and other similar parameters in silico rather than in vitro.
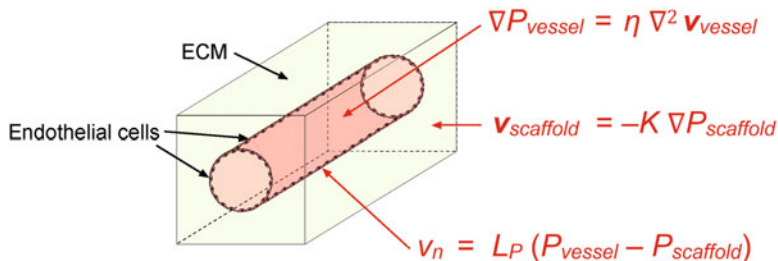
Fig. 7 Computational models of forces and flows in an endothelialized microfluidic ECM. Flow within the ECM, within the lumen, and across the endothelium is modeled with Darcy's law, the Navier-Stokes equation, and Starling's law, respectively. Shown are simplified versions of the Navier-Stokes equation and Starling's law that neglect inertial and oncotic terms, respectively. $P_{scaffold}$, pore pressure within ECM; P_{vessel}, fluid pressure within vessel lumen (equivalent to P_{lumen} in Fig. 5); $v_{scaffold}$, fluid velocity within ECM; v_{vessel}, fluid velocity within vessel lumen; v_n, trans-endothelial fluid velocity; η, viscosity of pore fluid; K, ECM hydraulic permeability; L_P, endothelial hydraulic conductivity

Of course, the computationally optimized design must ultimately be validated experimentally, but using computational models as a screening tool can greatly reduce the number of required experiments (Arrigoni et al. 2016).

Computational models of microfluidic ECM typically consist of modeling fluid and/or solute transport and mechanical deformation with finite-element analysis software (e.g., COMSOL Multiphysics, ANSYS, FEBio) (Fig. 7). Fluid transport within the matrix itself and in a vessel can be treated separately with Darcy's law and the Navier-Stokes equation, respectively. Since microfluidic systems typically operate at Reynolds numbers much smaller than one, the inertial term in the Navier-Stokes equation is often neglected. Coupling of flows at the vessel wall depends on the hydraulic properties of the interface. The transmural flow speed is a function of the transmural pressure, the transmural osmotic pressure difference, and the hydraulic conductivity of the wall, as given by Starling's law of filtration (Yuan and Rigor 2011). In practice, the osmotic pressure difference is sometimes neglected, so that transmural flow is proportional to the transmural pressure. Setting input and output pressures to equal chosen values fully defines the flow problem, which allows solving for the flow field. For a scaffold with unseeded channels, it is easier to model the entire system with Darcy's law plus a Brinkman term, in which the channel is considered to be a porous medium with a much larger hydraulic permeability than in the matrix itself. Once the flow field is obtained, solute transport can be modeled with the reaction-convection-diffusion equation and appropriate boundary conditions (Choi et al. 2007). At a vessel wall, transmural solute flux is assumed to be a product of the transmural solute concentration difference and an effective solute permeability coefficient (Yuan and Rigor 2011). Material constants, such as the matrix permeability and the vascular hydraulic conductivity, are either measured separately (e.g., in bulk ECM) or estimated from the literature.

Mechanical deformation of the ECM is modeled computationally by assuming that the matrix is an isotropic solid. Elastic moduli are usually measured separately

with standard mechanical testing (e.g., with a rheometer). Solving these models yields the displacement, stress, and strain fields in the scaffold. Less commonly, the ECM is modeled as a poroelastic solid, which couples the interstitial fluid pressure (which itself is modeled with Darcy's law) and the deformation of the solid. Whether the computational models analyze transport or mechanics or both, standard procedures to test model convergence and sensitivity to starting values should be applied.

Use of computational models to optimize microfluidic design requires one to explicitly state what is being optimized and what is held constant. These studies have been motivated by the use of such ECM scaffolds for perfusion of engineered tissues. As such, the desired optimization is often the minimization of a vascular parameter, such as the volume occupied by the vessels, which enables a greater fraction of the scaffold to be devoted to parenchymal cells (Truslow and Tien 2011). Other plausible optimization strategies include minimizing the pressure difference required to maintain oxygen concentration above a given threshold throughout the tissue, minimizing the heterogeneity of flow velocity and/or shear stress among vascular segments, maximizing the vascular surface area for a given network topology, and maximizing the transmural pressure for a given lymphatic pressure (Barber and Emerson 2010; Janakiraman et al. 2007; Truslow et al. 2009; Wang and Hsu 2006). To reduce the computational burden, simple and symmetric vascular geometries (e.g., arrays of regularly spaced vessels) are typically analyzed. Modeling entire microvascular networks is substantially more computationally intensive, and the parameter space is also much broader. For network design, one often starts with geometries that mimic those found in vivo and that obey phenomenological anatomical relations, such as Murray's law, which relates the diameters of afferent and efferent vessels at a junction (Barber and Emerson 2010; Hoganson et al. 2010).

Microfluidic ECMs in Models of Epithelial Ducts

Microfluidic ECM can also be used to form open and/or blind-ended epithelial tubes. Such structures form a variety of transport systems in vivo, such as the collecting duct tree in the kidney and the milk-secreting ductal tree in the mammary gland. Compared to microfluidic vascularization, the formation of epithelial tubes in microfluidic ECM is less well-studied. Most efforts to date have focused on reproducing epithelial geometry without requiring the full set of organ-specific epithelial functions.

Similarities and Differences with Endothelialization

Although epithelial ducts exhibit the tubular geometries of microvessels, they have unique aspects that distinguish them from microvessels. First, epithelial cells originate from endoderm or ectoderm, while endothelial cells arise from mesoderm. (To avoid confusion, endothelial cells are not referred to as "ECs" in this section.)

Although epithelial and endothelial cells both form monolayers, the mesenchymal nature of endothelial cells generally leads to a more migratory phenotype. Epithelial cells are often limited in their migration in a microfluidic ECM and can grow as tight colonies instead of as well-dispersed cells.

Second, epithelium contains significantly tighter junctions than endothelium does (with the notable exception of the BBB). The looser junctions between endothelial cells allow passive exchange of fluids and solutes to supply tissues with nutrients and oxygen. In contrast, epithelial tight junctions form a highly regulated "fence" that greatly restricts trans-epithelial transport. Macromolecular solutes that are suitable for probing the barrier properties of engineered microvessels are too large for use in engineered epithelial tubes. Low-molecular-weight solutes, such as Lucifer Yellow and fluorescein, are better suited for the latter. Measurement of trans-epithelial electrical resistance can also give a quantitative picture of the epithelial barrier.

Third, epithelial ducts are arranged in fractal branching trees, in which large ducts bifurcate repeatedly into progressively smaller ductules or tubules. Each epithelial organ has a unique branching architecture, with characteristic branching angles, length ratios, and terminal structures (Kessel and Kardon 1979). In contrast, microvascular networks are highly interconnected, even in the lymphatic system. In many organs, the lymphatic capillaries are often arranged in a plexus rather than in a strict branching pattern (Breslin et al. 2018).

Fourth, epithelial cell culture presents some practical challenges not encountered in endothelial cell culture. Epithelial cells tend to be more finicky in their growth and often require specialized media formulations. For some epithelial cell types, optimal culture conditions have not yet been developed, and cultures can senesce after many fewer population doublings than endothelial cells typically do. Even when they can be successfully passaged, epithelial cells can drift in culture and lose their characteristic tight barrier.

Formation of Epithelial Tubes in Microfluidic ECM

Techniques for microfluidic vascularization can be readily adapted to form epithelial tubes in vitro. In general, a suspension of epithelial cells is introduced into the channel; once cells have adhered, remaining non-adherent cells are removed by reversing the flow. Seeded cells often grow as tight colonies on the channel surface. Under appropriate culture conditions, these colonies can expand and eventually merge to form a thick-walled epithelial tube.

This approach can be used to form epithelial tubes that model ducts from a variety of tissues. In the kidney, distinct types of ducts constitute the epithelial portion of the nephron, which is the structure targeted in microfluidic models. Early work used single microfluidic channels in a type I collagen gel to form single tubules from Madin-Darby canine kidney (MDCK) cells (Fig. 8a) (Bogorad and Searson 2016). Although MDCK cells are derived from renal tubules, the precise segment of origin (e.g., proximal tubule) is unclear, and MDCK cells are used here as an all-purpose immortalized epithelial cell. Subsequent work used renal epithelial cells of human
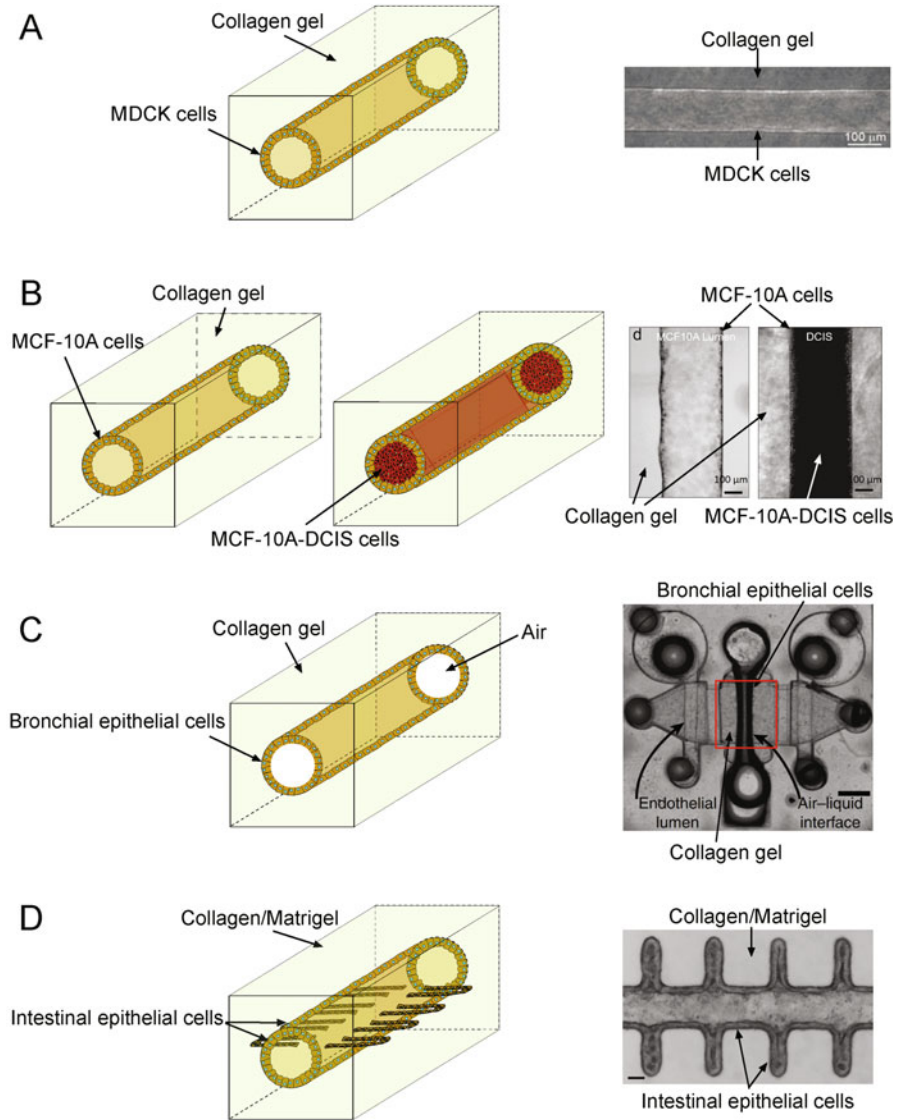
Fig. 8 Microfluidic engineering of epithelial structures. (**a**) Renal ducts. (Reproduced with permission from Bogorad and Searson 2016). (**b**) Mammary ducts. (Reproduced with permission from Ayuso et al. 2018). (**c**) Bronchioles. (Reproduced under a Creative Commons CC BY license from Barkal et al. 2017). Schematic drawing refers to the region outlined in red. (**d**) Intestine/gut. (Reproduced with permission from Nikolaev et al. 2020). Scale bars refer to 500 μm in (**c**) and 50 μm in (**d**)

origin in collagen- or gelatin/fibrin-based microfluidic ECMs that contained micro-molded or 3D-printed channels, respectively (Homan et al. 2016; Lin et al. 2019; Weber et al. 2016). These renal tubule models express renal epithelial cell markers

E-cadherin and aquaporin-1 and exhibit the native polarity of the renal proximal tubule. Engineered renal tubes display appropriate tight barrier function and can be used to investigate trans-epithelial drug transport and renal damage from hyperglycemia and nephrotoxic drugs (Adler et al. 2016; Bogorad and Searson 2016; Lin et al. 2019). A combination of engineered liver-on-a-chip with a perfusable proximal tubule enables study of liver-induced renal toxicity (Chang et al. 2017).

In the mammary gland, epithelial tubes are arranged in ductal-lobular units within a fibrous or fatty stroma, depending on the species. Both micromolding and viscous fingering techniques have been used to engineer microfluidic mammary epithelial ducts, with essentially all studies relying on immortalized mammary cell lines such as MCF-10A and MCF-7 (Fig. 8b) (Bischel et al. 2015; Morgan et al. 2018). Mammary epithelial tubes can be surrounded by a stromal cell-laden scaffold that contains mammary fibroblasts (Bischel et al. 2015), adipose stromal cells (Morgan et al. 2019), or natural killer lymphocytes (Ayuso et al. 2019). They can be used to evaluate estrogen receptor (ER)-mediated proliferation in ER+ breast cancer (Morgan et al. 2019; Morgan et al. 2018). The engineered tubes can also be backfilled with transformed mammary epithelial cells to model ductal carcinoma in situ (Ayuso et al. 2018; Bischel et al. 2015). In the absence of a non-transformed epithelial monolayer, transformed epithelial cells form dense aggregates of breast cancer cells that eventually invade into the surrounding ECM (Tien et al. 2012). These invasive "micro-tumors" can then escape into a neighboring lymphatic-like cavity, in a process that resembles intravasation (Rabie et al. 2021; Tien et al. 2021; Tien et al. 2020). Adipocytes and adipose-derived stem cells can be embedded into the ECM to engineer an adipose stroma through which breast cancer cells can invade and escape (Dance et al. 2022). Additional information about ECM-based in vitro cancer models can be obtained from the chapter by Ramos et al. in this handbook.

Other epithelial tissues are less commonly studied and are ripe for exploration. Microfluidic collagen gels can be used to form an airway epithelial tube (a "bronchiole") with an air-filled lumen (Fig. 8c) (Barkal et al. 2017). Inoculation of the airway space with a fungal pathogen results in airway inflammation. Laser ablation of a collagen/Matrigel ECM can form wavy, perfusable microchannels that template the formation of intestinal crypt-like structures ("mini-guts") (Fig. 8d) (Nikolaev et al. 2020). As in the bronchiole, the introduction of pathogens into the apical side of the mini-gut epithelium results in inflammation within the epithelium. Such models have been used to assess long-term parasitic infection of intestinal epithelium.

Greater physiological complexity can be obtained by forming epithelial tubes in close proximity to perfusable microvessels in the same ECM. In many epithelial tissues, the microvasculature does not exist solely to provide nutrients but serves as an integral partner in the transport processes that characterize the tissue. Engineered renal tubules that are located near perfused microvessels can model proximal tubule filtration and reabsorption (Lin et al. 2019; Rayner et al. 2018). Similarly, bronchioles that are located near perfused microvessels can model inflammatory communication between the two compartments, in which bronchiole-derived signals induce

leukocyte extravasation from the vessel lumen into the ECM that separates epithelial and endothelial tubes.

Design Considerations for Epithelialization

Much of the work on using microfluidic ECM for epithelial tubes is qualitative and based on trial and error, with quantitative design principles poorly explored. For instance, what properties of a protein-based scaffold promote stability of an epithelial lumen? How do the stiffness, pore size, and porosity of the ECM control epithelial cell adhesion and proliferation to form a confluent 3D duct? Given that epithelium in vivo normally exists in a low-flow, low-pressure environment, do physical stresses play an important role in promoting the formation of epithelial tubes? To what extent do the physiological ductal diameters need to be replicated to obtain a desired set of epithelial functions in vitro? To answer these questions, it may be important to understand how the active transport pathways across epithelium are modified by these elements of the physical microenvironment.

Conclusions

Protein-based microfluidic ECM models have provided unique capabilities in biomedical applications. Their ability to be readily perfused without relying on biologically-driven tubulogenesis makes this class of biomaterials particularly well-suited for modeling physiological and pathological processes in which access to a lumen is required. Such processes often involve fluid and/or solute transport in vessels and in their surrounding tissues. Moreover, these models can be used to analyze microfluidic designs in a small-scale format before they are incorporated into engineered tissues of clinically relevant size. Ever since the first description of a microfluidic biomaterial nearly two decades ago (Stroock and Cabodi 2006), numerous studies have applied this strategy to materials of different compositions and network geometries, with applications as varied as modeling the vascular and epithelial barrier and understanding the role of microvascular obstruction in the sequelae of hematological disease.

Much of the progress to date has relied upon single-layered vessels or epithelial tubes within a ECM of uniform composition as the basic biological unit. For understanding transmural transport, the diameter of the tube does not need to precisely match that of the in vivo structure that it is intended to model. As mentioned in this chapter, the engineered system can provide advantages in visualizing transport processes that are difficult to observe in vivo. Nevertheless, it is likely that further development of these microfluidic models will require them to adhere more closely to native microfluidic geometries and include a surrounding layer of mural cells (e.g., myoepithelial cells for glandular ducts). To what extent a tortuous open network (e.g., 3D microvasculature) can be simplified without loss of its geometry-specific function is an open question. The answer to this question will help indicate which features of complex in vivo 3D networks are essential to retain for in vitro modeling.

Studies in existing microfluidic models have already revealed similarities and differences between the functions obtained in vitro and observed in vivo. In general, qualitative responses to a perturbation (e.g., breakdown of the vascular barrier after addition of an inflammatory compound) are similar in vitro and in vivo. Quantitative responses, as measured by physiological assays, often differ substantially. The origins of these quantitative differences remain unclear; peculiarities of the in vitro environment, such as supra-physiological oxygen levels and the accompanying high levels of oxidative stress, may be partly responsible. Understanding how differences in the in vitro and in vivo environments contribute to the differences in model and actual tissue function is likely to drive further studies in this area.

As several chapters in this handbook show, 3D printing has risen to become the method of choice among many research groups for creating microfluidic scaffolds. This development will certainly continue, although older methods that use PDMS molds and soft lithography have complementary strengths and, depending on the application, may be a better choice.

Progress in microfluidic models has largely achieved Vacanti's original vision (Kaihara et al. 2000): the creation of microvascular networks that replicate an in silico microfluidic design is not only possible but now can be routinely achieved by a variety of methods. Further progress is likely to lead to the creation of microvascular networks that are even further integrated with tissue function. For instance, much of the work to date has incorporated microvessels in a microfluidic ECM as a means to perfuse the tissue. In many organs, such as the kidney and lungs, the vasculature is inextricably intertwined with the parenchymal compartment. Building microfluidic scaffolds that can faithfully model the blood-air barrier, gas transport, the formation of ultrafiltrate and urine, or the incorporation of plasma lipids into secreted milk remains a challenge for the enterprising young researcher.

Advancements in forming organ-specific vascular and epithelial models are almost certainly required to realize these aims. For instance, creation of a functional glomerulus will not only require the ability to replicate the close apposition of endothelial and glomerular epithelial cell monolayers but will also need the endothelial cells to adopt the unique phenotype found in glomerular capillaries. The set of microenvironmental signals that are sufficient to coax endothelial cells into displaying organ-specific phenotypes is unclear. Diverse approaches from developmental biology, induced pluripotent stem cell engineering, and organ-specific angiocrine and matrix biology may be helpful. Recent work on the formation of a functional blood-brain barrier in microfluidic ECM with stem cell-derived ECs demonstrates the possibilities (Linville et al. 2019).

Cross-References

▶ Protein-based Materials as Cancer in Vitro Models
▶ Protein-derived 3D Bioprinted Models for Tissue Engineering
▶ Proteins and Polypeptides as Biomaterials Inks for 3D Printing

References

Adler M, Ramm S, Hafner M, Muhlich JL, Gottwald EM, Weber E, Jaklic A, Ajay AK, Svoboda D, Auerbach S, Kelly EJ, Himmelfarb J, Vaidya VS. A quantitative approach to screen for nephrotoxic compounds *in vitro*. J Am Soc Nephrol. 2016;27:1015–28.

Arakawa C, Gunnarsson C, Howard C, Bernabeu M, Phong K, Yang E, DeForest CA, Smith JD, Zheng Y. Biophysical and biomolecular interactions of malaria-infected erythrocytes in engineered human capillaries. Sci Adv. 2020;6:eaay7243.

Arrigoni C, Bongio M, Talò G, Bersini S, Enomoto J, Fukuda J, Moretti M. Rational design of prevascularized large 3D tissue constructs using computational simulations and biofabrication of geometrically controlled microvessels. Adv Healthcare Mater. 2016;5:1617–26.

Ayuso JM, Gillette A, Lugo-Cintrón K, Acevedo-Acevedo S, Gomez I, Morgan M, Heaster T, Wisinski KB, Palecek SP, Skala MC, Beebe DJ. Organotypic microfluidic breast cancer model reveals starvation-induced spatial-temporal metabolic adaptations. EBioMedicine. 2018;37:144–57.

Ayuso JM, Truttschel R, Gong MM, Humayun M, Virumbrales-Munoz M, Vitek R, Felder M, Gillies SD, Sondel P, Wisinski KB, Patankar M, Beebe DJ, Skala MC. Evaluating natural killer cell cytotoxicity against solid tumors using a microfluidic model. Oncoimmunology. 2019;8:1553477.

Badylak SF, Taylor D, Uygun K. Whole-organ tissue engineering: decellularization and recellularization of three-dimensional matrix scaffolds. Annu Rev Biomed Eng. 2011;13:27–53.

Barber RW, Emerson DR. Biomimetic design of artificial micro-vasculatures for tissue engineering. Altern Lab Anim. 2010;38:S67–79.

Barkal LJ, Procknow CL, Álvarez-García YR, Niu M, Jiménez-Torres JA, Brockman-Schneider RA, Gern JE, Denlinger LC, Theberge AB, Keller NP, Berthier E, Beebe DJ. Microbial volatile communication in human organotypic lung models. Nat Commun. 2017;8:1770.

Bettinger CJ, Cyr KM, Matsumoto A, Langer R, Borenstein JT, Kaplan DL. Silk fibroin microfluidic devices. Adv Mater. 2007;19:2847–50.

Bischel LL, Lee S-H, Beebe DJ. A practical method for patterning lumens through ECM hydrogels via viscous finger patterning. J Lab Autom. 2012;17:96–103.

Bischel LL, Beebe DJ, Sung KE. Microfluidic model of ductal carcinoma in situ with 3D, organotypic structure. BMC Cancer. 2015;15:12.

Bogorad MI, Searson PC. Real-time imaging and quantitative analysis of doxorubicin transport in a perfusable microvessel platform. Integr Biol. 2016;8:976–84.

Borenstein JT, Terai H, King KR, Weinberg EJ, Kaazempur-Mofrad MR, Vacanti JP. Microfabrication technology for vascularized tissue engineering. Biomed Microdevices. 2002;4:167–75.

Breslin JW, Yang Y, Scallan JP, Sweat RS, Adderley SP, Murfee WL. Lymphatic vessel network structure and physiology. Compr Physiol. 2018;9:207–99.

Cabodi M, Choi NW, Gleghorn JP, Lee CS, Bonassar LJ, Stroock AD. A microfluidic biomaterial. J Am Chem Soc. 2005;127:13788–9.

Chan KLS, Khankhel AH, Thompson RL, Coisman BJ, Wong KHK, Truslow JG, Tien J. Crosslinking of collagen scaffolds promotes blood and lymphatic vascular stability. J Biomed Mater Res A. 2014;102:3186–95.

Chang S-Y, Weber EJ, Sidorenko VS, Chapron A, Yeung CK, Gao C, Mao Q, Shen D, Wang J, Rosenquist TA, Dickman KG, Neumann T, Grollman AP, Kelly EJ, Himmelfarb J, Eaton DL. Human liver-kidney model elucidates the mechanisms of aristolochic acid nephrotoxicity. JCI Insight. 2017;2:e95978.

Choi NW, Cabodi M, Held B, Gleghorn JP, Bonassar LJ, Stroock AD. Microfluidic scaffolds for tissue engineering. Nat Mater. 2007;6:908–15.

Chrobak KM, Potter DR, Tien J. Formation of perfused, functional microvascular tubes in vitro. Microvasc Res. 2006;71:185–96.

Dance YW, Meshulam T, Seibel AJ, Obenreder MC, Layne MD, Nelson CM, Tien J. Adipose stroma accelerates the invasion and escape of human breast cancer cells from an engineered microtumor. Cell Mol Bioeng. 2022;15:15–29.

Enrico A, Voulgaris D, Östmans R, Sundaravadivel N, Moutaux L, Cordier A, Niklaus F, Herland A, Stemme G. Three dimensional microvascularized tissue models by laser-based cavitation molding of collagen. Adv Mater. 2022:e2109823.

Galie PA, Nguyen D-HT, Choi CK, Cohen DM, Janmey PA, Chen CS. Fluid shear stress threshold regulates angiogenic sprouting. Proc Natl Acad Sci U S A. 2014;111:7968–73.

Gershlak JR, Hernandez S, Fontana G, Perreault LR, Hansen KJ, Larson SA, Binder BYK, Dolivo DM, Yang T, Dominko T, Rolle MW, Weathers PJ, Medina-Bolivar F, Cramer CL, Murphy WL, Gaudette GR. Crossing kingdoms: using decellularized plants as perfusable tissue engineering scaffolds. Biomaterials. 2017;125:13–22.

Golden AP, Tien J. Fabrication of microfluidic hydrogels using molded gelatin as a sacrificial element. Lab Chip. 2007;7:720–5.

Grover WH, Ivester RHC, Jensen EC, Mathies RA. Development and multiplexed control of latching pneumatic valves using microfluidic logical structures. Lab Chip. 2006;6:623–31.

Hinton TJ, Jallerat Q, Palchesko RN, Park JH, Grodzicki MS, Shue H-J, Ramadan MH, Hudson AR, Feinberg AW. Three-dimensional printing of complex biological structures by freeform reversible embedding of suspended hydrogels. Sci Adv. 2015;1:e1500758.

Hoganson DM, Pryor HI 2nd, Spool ID, Burns OH, Gilmore JR, Vacanti JP. Principles of biomimetic vascular network design applied to a tissue-engineered liver scaffold. Tissue Eng A. 2010;16:1469–77.

Homan KA, Kolesky DB, Skylar-Scott MA, Herrmann J, Obuobi H, Moisan A, Lewis JA. Bioprinting of 3D convoluted renal proximal tubules on perfusable chips. Sci Rep. 2016;6:34845.

Huh D, Matthews BD, Mammoto A, Montoya-Zavala M, Hsin HY, Ingber DE. Reconstituting organ-level lung functions on a chip. Science. 2010;328:1662–8.

Ilina O, Bakker G-J, Vasaturo A, Hofmann RM, Friedl P. Two-photon laser-generated microtracks in 3D collagen lattices: principles of MMP-dependent and -independent collective cancer cell invasion. Phys Biol. 2011;8:015010.

Janakiraman V, Mathur K, Baskaran H. Optimal planar flow network designs for tissue engineered constructs with built-in vasculature. Ann Biomed Eng. 2007;35:337–47.

Jiménez-Torres JA, Peery SL, Sung KE, Beebe DJ. LumeNEXT: a practical method to pattern luminal structures in ECM gels. Adv Healthcare Mater. 2016;5:198–204.

Kaihara S, Borenstein J, Koka R, Lalan S, Ochoa ER, Ravens M, Pien H, Cunningham B, Vacanti JP. Silicon micromachining to tissue engineer branched vascular channels for liver fabrication. Tissue Eng. 2000;6:105–17.

Kessel RG, Kardon RH. Tissues and Organs: A Text-Atlas of Scanning Electron Microscopy. San Francisco: W. H. Freeman; 1979. p. 317.

Kolesky DB, Truby RL, Gladman AS, Busbee TA, Homan KA, Lewis JA. 3D bioprinting of vascularized, heterogeneous cell-laden tissue constructs. Adv Mater. 2014;26:3124–30.

Lee A, Hudson AR, Shiwarski DJ, Tashman JW, Hinton TJ, Yerneni S, Bliley JM, Campbell PG, Feinberg AW. 3D bioprinting of collagen to rebuild components of the human heart. Science. 2019;365:482–7.

Leung AD, Wong KHK, Tien J. Plasma expanders stabilize human microvessels in microfluidic scaffolds. J Biomed Mater Res A. 2012;100:1815–22.

Li X, Xia J, Nicolescu CT, Massidda MW, Ryan TJ, Tien J. Engineering of microscale vascularized fat that responds to perfusion with lipoactive hormones. Biofabrication. 2019;11:014101.

Lin NYC, Homan KA, Robinson SS, Kolesky DB, Duarte N, Moisan A, Lewis JA. Renal reabsorption in 3D vascularized proximal tubule models. Proc Natl Acad Sci U S A. 2019;116:5399–404.

Linville RM, Boland NF, Covarrubias G, Price GM, Tien J. Physical and chemical signals that promote vascularization of capillary-scale channels. Cell Mol Bioeng. 2016;9:73–84.

Linville RM, DeStefano JG, Sklar MB, Chu C, Walczak P, Searson PC. Modeling hyperosmotic blood-brain barrier opening within human tissue-engineered in vitro brain microvessels. J Cereb Blood Flow Metab. 2020;40:1517–32.

Linville RM, Komin A, Lan X, DeStefano JG, Chu C, Liu G, Walczak P, Hristova K, Searson PC. Reversible blood-brain barrier opening utilizing the membrane active peptide melittin *in vitro* and *in vivo*. Biomaterials. 2021;275:120942.

Linville RM, DeStefano JG, Sklar MB, Xu Z, Farrell AM, Bogorad MI, Chu C, Walczak P, Cheng L, Mahairaki V, Whartenby KA, Calabresi PA, Searson PC. Human iPSC-derived blood-brain barrier microvessels: validation of barrier function and endothelial cell behavior. Biomaterials. 2019;190-191:24–37.

McDonald JC, Whitesides GM. Poly(dimethylsiloxane) as a material for fabricating microfluidic devices. Acc Chem Res. 2002;35:491–9.

Melin J, Quake SR. Microfluidic large-scale integration: the evolution of design rules for biological automation. Annu Rev Biophys Biomol Struct. 2007;36:213–31.

Miller JS, Stevens KR, Yang MT, Baker BM, Nguyen D-HT, Cohen DM, Toro E, Chen AA, Galie PA, Yu X, Chaturvedi R, Bhatia SN, Chen CS. Rapid casting of patterned vascular networks for perfusable engineered three-dimensional tissues. Nat Mater. 2012;11:768–74.

Morgan MM, Arendt LM, Alarid ET, Beebe DJ, Johnson BP. Mammary adipose stromal cells derived from obese women reduce sensitivity to the aromatase inhibitor anastrazole in an organotypic breast model. FASEB J. 2019;33:8623–33.

Morgan MM, Livingston MK, Warrick JW, Stanek EM, Alarid ET, Beebe DJ, Johnson BP. Mammary fibroblasts reduce apoptosis and speed estrogen-induced hyperplasia in an organotypic MCF7-derived duct model. Sci Rep. 2018;8:7139.

Nelson CM, Tien J. Microstructured extracellular matrices in tissue engineering and development. Curr Opin Biotechnol. 2006;17:518–23.

Nelson CM, Inman JL, Bissell MJ. Three-dimensional lithographically defined organotypic tissue arrays for quantitative analysis of morphogenesis and neoplastic progression. Nat Protoc. 2008;3:674–8.

Nguyen D-HT, Stapleton SC, Yang MT, Cha SS, Choi CK, Galie PA, Chen CS. Biomimetic model to reconstitute angiogenic sprouting morphogenesis in vitro. Proc Natl Acad Sci U S A. 2013;110:6712–7.

Nikolaev M, Mitrofanova O, Broguiere N, Geraldo S, Dutta D, Tabata Y, Elci B, Brandenberg N, Kolotuev I, Gjorevski N, Clevers H, Lutolf MP. Homeostatic mini-intestines through scaffold-guided organoid morphogenesis. Nature. 2020;585:574–8.

Ohtani O, Kikuta A, Ohtsuka A, Taguchi T, Murakami T. Microvasculature as studied by the microvascular corrosion casting/scanning electron microscope method. I. Endocrine and digestive system. Arch Histol Jpn. 1983;46:1–42.

Ostrowski MA, Huang NF, Walker TW, Verwijlen T, Poplawski C, Khoo AS, Cooke JP, Fuller GG, Dunn AR. Microvascular endothelial cells migrate upstream and align against the shear stress field created by impinging flow. Biophys J. 2014;106:366–74.

Ott HC, Matthiesen TS, Goh S-K, Black LD, Kren SM, Netoff TI, Taylor DA. Perfusion-decellularized matrix: using nature's platform to engineer a bioartificial heart. Nat Med. 2008;14:213–21.

Price GM, Tien J. Subtractive methods for forming microfluidic gels of extracellular matrix proteins. In: Bhatia SN, Nahmias Y, editors. Microdevices in Biology and Engineering. Boston: Artech House; 2009. p. 235–48.

Price GM, Tien J. Methods for forming human microvascular tubes in vitro and measuring their macromolecular permeability. In: Khademhosseini A, Suh K-Y, Zourob M, editors. Biological Microarrays (Methods in Molecular Biology, vol 671). Totowa: Humana Press; 2011. p. 281–93.

Price GM, Wong KHK, Truslow JG, Leung AD, Acharya C, Tien J. Effect of mechanical factors on the function of engineered human blood microvessels in microfluidic collagen gels. Biomaterials. 2010;31:6182–9.

Price GM, Chu KK, Truslow JG, Tang-Schomer MD, Golden AP, Mertz J, Tien J. Bonding of macromolecular hydrogels using perturbants. J Am Chem Soc. 2008;130:6664–5.

Qiu Y, Ahn B, Sakurai Y, Hansen CE, Tran R, Mimche PN, Mannino RG, Ciciliano JC, Lamb TJ, Joiner CH, Ofori-Acquah SF, Lam WA. Microvasculature-on-a-chip for the long-term study of endothelial barrier dysfunction and microvascular obstruction in disease. Nat Biomed Eng. 2018;2:453–63.

Rabie EM, Zhang SX, Kourouklis AP, Kilinc AN, Simi AK, Radisky DC, Tien J, Nelson CM. Matrix degradation and cell proliferation are coupled to promote invasion and escape from an engineered human breast microtumor. Integr Biol. 2021;13:17–29.

Raub CB, Suresh V, Krasieva T, Lyubovitsky J, Mih JD, Putnam AJ, Tromberg BJ, George SC. Noninvasive assessment of collagen gel microstructure and mechanics using multiphoton microscopy. Biophys J. 2007;92:2212–22.

Rayner SG, Phong KT, Xue J, Lih D, Shankland SJ, Kelly EJ, Himmelfarb J, Zheng Y. Reconstructing the human renal vascular-tubular unit in vitro. Adv Healthcare Mater. 2018;7:e1801120.

Song YS, Lin RL, Montesano G, Durmus NG, Lee G, Yoo S-S, Kayaalp E, Haeggström E, Khademhosseini A, Demirci U. Engineered 3D tissue models for cell-laden microfluidic channels. Anal Bioanal Chem. 2009;395:185–93.

Stroock AD, Cabodi M. Microfluidic biomaterials. MRS Bull. 2006;31:114–9.

Tang MD, Golden AP, Tien J. Molding of three-dimensional microstructures of gels. J Am Chem Soc. 2003;125:12988–9.

Thompson RL, Margolis EA, Ryan TJ, Coisman BJ, Price GM, Wong KHK, Tien J. Design principles for lymphatic drainage of fluid and solutes from collagen scaffolds. J Biomed Mater Res A. 2018;106:106–14.

Tien J. Microfluidic approaches for engineering vasculature. Curr Opin Chem Eng. 2014;3:36–41.

Tien J, Nelson CM. Microstructured extracellular matrices in tissue engineering and development: an update. Ann Biomed Eng. 2014;42:1413–23.

Tien J, Dance YW. Microfluidic biomaterials. Adv Healthcare Mater. 2021;10:2001028.

Tien J, Truslow JG, Nelson CM. Modulation of invasive phenotype by interstitial pressure-driven convection in aggregates of human breast cancer cells. PLoS One. 2012;7:e45191.

Tien J, Dance YW, Ghani U, Seibel AJ, Nelson CM. Interstitial hypertension suppresses escape of human breast tumor cells *via* convection of interstitial fluid. Cell Mol Bioeng. 2021;14:147–59.

Tien J, Ghani U, Dance YW, Seibel AJ, Karakan MC, Ekinci KL, Nelson CM. Matrix pore size governs escape of human breast cancer cells from a microtumor to an empty cavity. iScience. 2020;23:101673.

Truslow JG, Tien J. Perfusion systems that minimize vascular volume fraction in engineered tissues. Biomicrofluidics. 2011;5:022201.

Truslow JG, Price GM, Tien J. Computational design of drainage systems for vascularized scaffolds. Biomaterials. 2009;30:4435–43.

Wang G-J, Hsu Y-F. Structure optimization of microvascular scaffolds. Biomed Microdevices. 2006;8:51–8.

Weber EJ, Chapron A, Chapron BD, Voellinger JL, Lidberg KA, Yeung CK, Wang Z, Yamaura Y, Hailey DW, Neumann T, Shen DD, Thummel KE, Muczynski KA, Himmelfarb J, Kelly EJ. Development of a microphysiological model of human kidney proximal tubule function. Kidney Int. 2016;90:627–37.

Wiedeman MP. Architecture. In: Renkin EM, Michel CC, editors. Handbook of Physiology; Section 2: The Cardiovascular System. IV: Microcirculation. Bethesda: American Physiological Society; 1984. p. 11–40.

Wong KHK, Truslow JG, Tien J. The role of cyclic AMP in normalizing the function of engineered human blood microvessels in microfluidic collagen gels. Biomaterials. 2010;31:4706–14.

Wong KHK, Truslow JG, Khankhel AH, Tien J. Biophysical mechanisms that govern the vascularization of microfluidic scaffolds. In: Brey EM, editor. Vascularization: Regenerative Medicine and Tissue Engineering. Boca Raton: CRC Press; 2014. p. 109–24.

Wong KHK, Truslow JG, Khankhel AH, Chan KLS, Tien J. Artificial lymphatic drainage systems for vascularized microfluidic scaffolds. J Biomed Mater Res A. 2013;101:2181–90.

Yuan SY, Rigor RR. In: Granger DN, Granger JP, editors. Regulation of Endothelial Barrier Function. San Rafael: Morgan & Claypool Life Sciences; 2011. p. 146.

Zheng Y, Chen J, Craven M, Choi NW, Totorica S, Diaz-Santana A, Kermani P, Hempstead B, Fischbach-Teschl C, López JA, Stroock AD. In vitro microvessels for the study of angiogenesis and thrombosis. Proc Natl Acad Sci U S A. 2012;109:9342–7.

Zweifach BW. Microcirculation. Annu Rev Physiol. 1973;35:117–50.